A Synaptic Corollary Discharge Signal Suppresses Midbrain Visual Processing During Saccade-Like Locomotion

Mir Ahsan Ali[1,#], Katharina Lischka[1,#], Stephanie J. Preuss[2,4], Chintan A. Trivedi[2,5], Johann H. Bollmann[1,2,3]

ABSTRACT

In motor control, the brain not only sends motor commands to the periphery, but it also generates concurrent internal signals known as corollary discharge that influence the processing of sensory information around the time of movement. Corollary discharge signals are important for the brain to identify sensory input arising from self-motion and to compensate for it, but the underlying mechanisms remain unclear. Using whole-cell patch clamp recordings from single neurons in the optic tectum of zebrafish, we discovered an inhibitory synaptic signal which was temporally locked to spontaneous and visually driven swim patterns. This motor-related synaptic signal transiently suppressed tectal output and was appropriately timed to counteract visually driven excitatory input arising from the fish's own motion. High-resolution calcium imaging revealed brief, highly localized post-swim signals in the tectal neuropil, suggesting that corollary discharge enters the tectum in its most superficial layer. Our results demonstrate how spurious visual input is suppressed during self-motion by motor-related phasic inhibition in the tectum. This may help explain perceptual saccadic suppression observed in many species.

[1]Institute of Biology I, Faculty of Biology, University of Freiburg, 79104 Freiburg, Germany
[2]Max Planck Institute for Medical Research, 69120 Heidelberg, Germany
[3]Bernstein Center Freiburg, University of Freiburg, 79104 Freiburg, Germany
[4]Present Address: Springer Nature Group, Heidelberg, Germany
[5]Present Address: Dept Cell and Developmental Biology, University College London, London, United Kingdom
[#]equal contribution

Correspondence:
Dr. Johann Bollmann, University of Freiburg, Institute of Biology I, Hauptstrasse 1, 79104 Freiburg, Germany, E-mail: johann.bollmann@bio.uni-freiburg.de

INTRODUCTION

What signals run through the brain when a small, brisk movement, such as a saccade of the eyes, makes our gaze jump from one point to another? First, thousands of photoreceptors across the retina generate signals driven by the abrupt, global shift of the retinal image; the retinal circuitry further processes these signals and sends them to higher sensory areas[1]. Simultaneously, a second type of signal can be observed in areas downstream of the retina, occurring around the time of the rapid eye movement. These movement-associated signals, known as corollary discharge (CD), encode variables such as the timing, strength or direction of self-generated movements[2-6]. As a consequence, the nervous system can use CD signals as a flag to identify sensory signals arising from self-motion (reafference)[4] and account for them when processing and evaluating signals arising from external stimuli (exafference), which are ethologically more relevant.

Among various experimental demonstrations of CD signaling[2,6-9], recordings in the primate visual system show that the spiking activity of visual neurons both in visual cortical and subcortical areas[10-13] is transiently reduced during a saccade. This brief suppression likely contributes to the perceptual phenomenon of saccadic suppression, that is, the reduced perceptual sensitivity during saccadic eye movements. Another example is the fly visual system: here, during flight, visual neurons use CD signals in a subtractive computation to remove the visual input components caused by self-motion that would otherwise activate stabilizing visuomotor reflexes during flight[14,15], while, during walking, motor-related signals in these neurons may have course-stabilizing effects[16]. Collectively, experimental evidence has demonstrated that visual neurons are modulated during fast, saccade-like movements. In the vertebrate visual system, however, the underlying cellular and synaptic mechanisms remain poorly understood.

The zebrafish model offers new opportunities to investigate in the intact brain where and how motor-related signals modulate visual processing during intermittent, “saccade-like” locomotory sequences[17]. For locomotion, larval zebrafish typically use discrete swim bouts lasting 100-300 ms, interspersed with resting phases of 0.5 s to 1 s[18], much resembling the temporal characteristics of saccadic eye movement sequences when a primate scans a visual scene. Larval zebrafish are capable

hunters: they track and capture moving prey in a seconds-long, goal-driven sequence of visually guided swim bouts[19-21], wherein the onset of the next swim bout depends on appropriate visual feedback immediately following the previous one[21,22]. As the image of the surrounding world sweeps across the retina during each swim bout, a barrage of afferent inputs is expected to reach retinorecipient areas, likely obscuring signals that encode local, ethologically relevant visual stimuli, or inappropriately feeding into visual reflex pathways such as the optomotor response. Therefore, a CD-based transient suppression of visual sensitivity while it is moving should be advantageous for the larva: it would help filter out signals from the self-motion generated blur on the retina, and potentially sensitize the visual system for detecting local visual stimuli immediately after the swim bout. While in recent years, much has been learned about the visual response properties of neurons in the intact zebrafish brain[23], information about motor-related signals in retinorecipient areas is lacking.

Here, we discovered a swim-related CD signal in the main retinorecipient center, the optic tectum (homologous to the mammalian superior colliculus) during spontaneous and visually evoked swim bouts in larval zebrafish. Using targeted patch clamp recordings[24-26] in combination with bilateral tail motor nerve recordings[27,28], we found that many tectal neurons receive a phasic inhibitory synaptic input, temporally locked to the swim bout. Its timing matches that of excitatory input in the same cells in response to abrupt large-field visual motion stimuli associated with self-motion. Furthermore, we show that this inhibitory signal is sufficient to suppress visually evoked spike output from tectal neurons during visually driven fictive swimming. Collectively, our results demonstrate an effective CD mechanism in the developing visual system capable of transiently suppressing visual information processing during saccade-like locomotion.

RESULTS

Patch-clamp recordings reveal a motor-related voltage signal in tectal neurons

In the fully crossed retinotectal pathway of zebrafish, stimuli of different ethological relevance, such as small prey-like particles or dark expanding discs, generate different patterns of neuronal activity contralateral to the stimulated eye (Fig. 1A). These patterns are classified in intratectal circuitry, resulting in different patterns of output activity that are transmitted to downstream premotor areas. Here, they are translated into motor commands encoding different classes of swim bouts, directed toward or away from the visual object (Fig. 1A). Whether visual processing in the tectum is influenced by motor-related signals is, however, unknown. To investigate the impact of motor activity in the tectum, we performed two-photon-targeted patch-clamp recordings[29] from single tectal neurons and simultaneously recorded fictive motor activity bilaterally from the motor nerves of the tail muscles (Fig. 1B). We performed these recordings in the transgenic line *Tg(pou4f1-hsp70l:GFP)*[30]. In this line, GFP is expressed in neurons projecting to the ipsilateral reticular formation, the contralateral tectal hemisphere and local interneurons[31]. We recorded from both GFP-positive and GFP-negative cells in this line (compare Fig. 7). Furthermore, we visualized the dendritic branching pattern of the recorded neuron using sulforhodamine labeling (Figure 1C).

To search for possible CD signals in the tectum, we measured the membrane potential of individual neurons in current clamp while the larva performed spontaneous fictive swim bouts. Notably, we often observed a small, brief hyperpolarization occurring after the onset of a swim bout (Fig. 1D). We calculated the swim-triggered averages of voltage recordings in 21 cells, in which we measured membrane voltage while the larva exhibited spontaneous fictive swimming behavior. When aligned to swim onset, we observed a transient hyperpolarization of -1.57 ± 0.32 mV (n = 21 cells, mean ± SEM; Fig. 1E). The swim-related hyperpolarization was variable across cells: the average amplitude varied between 0.16 mV and -5.12 mV. This finding indicates that neurons in the tectum are modulated during spontaneous swimming, suggesting there is a CD signal relaying motor-information to this central visual processing center.

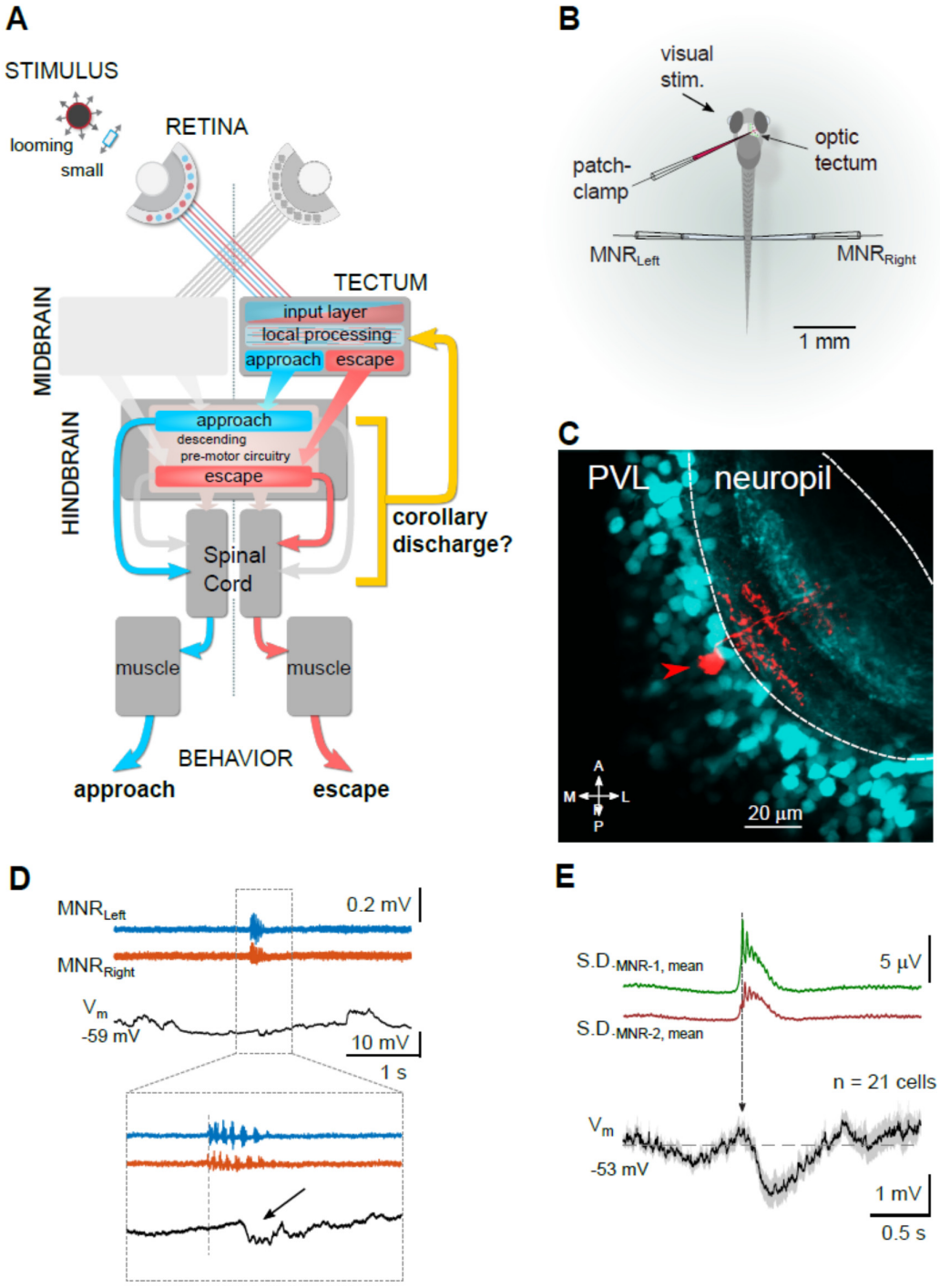

Figure 1. Patch-clamp recordings reveal a motor-related voltage signal in tectal neurons
(A) Schematic of the visuomotor pathway in larval zebrafish, including the retina, the optic tectum, hindbrain premotor circuits, spinal cord and axial tail muscles. Visual stimuli of different behavioral value (e.g. loom vs small, prey-like) are processed in the contralateral tectal hemisphere and trigger aversive (escape, red) or target-directed swims (approach, blue) through parallel pathways into the hindbrain pre-motor circuitry. Putative swim-related feedback signals may affect tectal visual processing during phases of swimming (corollary discharge, yellow).

(B) Recording configuration. Whole-cell patch clamp recording from a tectal neuron is combined with bilateral extracellular field recordings from tail motor nerves (MNR_{Left} and MNR_{Right}).
(C) Recorded tectal neuron (red) labeled with sulforhodamine-B via the patch pipette in *Tg(pou4f1-hsp70l:GFP)* transgenic background (cyan). PVL, periventricular cell body layer.
(D) Example recording of membrane voltage (V_m, black) in a tectal neuron during a spontaneous fictive swim bout (MNR_{Left}, MNR_{Right}, blue and red, respectively). Inset: Magnified view of swim event (onset indicated by dotted line). Note the associated, short hyperpolarization in the voltage trace (arrow).
(E) Swim-triggered average of voltage signals in tectal neurons (bottom, mean ± SEM; average across 21 individual, baseline-subtracted cell averages). V_m traces were aligned by the onset of swimming (vertical arrow), measured as the first burst in a fictive swim bout. Top: Standard deviation traces of motor nerve recordings (average from 330 swim events).

During spontaneous swim bouts, tectal neurons receive motor-related phasic inhibition

To investigate the cause of these motor-related voltage fluctuations, we performed measurements of synaptic currents in tectal neurons in voltage clamp to resolve putative inhibitory postsynaptic currents (IPSCs). We observed that in a majority of cells, a brief IPSC occurred immediately after a spontaneous swim bout (Fig. 2A). The IPSC was composed of a few individual current peaks and ended shortly after the swim bout. We calculated the charge integral as a measure of the strength of the synaptic input and measured the delay of the IPSC relative to swim onset (Fig. 2B). The charge histogram was multi-modal; it showed a peak around 0 pC (blue bars and dashed Gaussian fit in Fig. 2C), corresponding to cells in which no phasic IPSC was observed (n = 24). 32 cells, however, received phasic inhibitory synaptic input >0.8 pC after a swim bout (blue bars overlaid with magenta color, Fig. 2C). The delay between the onset of swimming and the onset of the IPSC was 124 ms ± 5 ms (mean ± SEM, n = 32; Figure 2D).

The cells in which we had measured a motor-related hyperpolarization signal (Fig. 1E) are a subset of these 56 cells. Therefore, we could compare the average hyperpolarization measured in current clamp in each cell with the average amount of inhibitory charge transfer measured in voltage clamp (Fig. 2E). We found that the transient drop in membrane voltage was correlated with the IPSC charge. We conclude that tectal cells receive a fast CD signal in form of a strong, phasic inhibitory synaptic input, which causes transient membrane hyperpolarization and could therefore modulate tectal cell activity during self-generated locomotion.

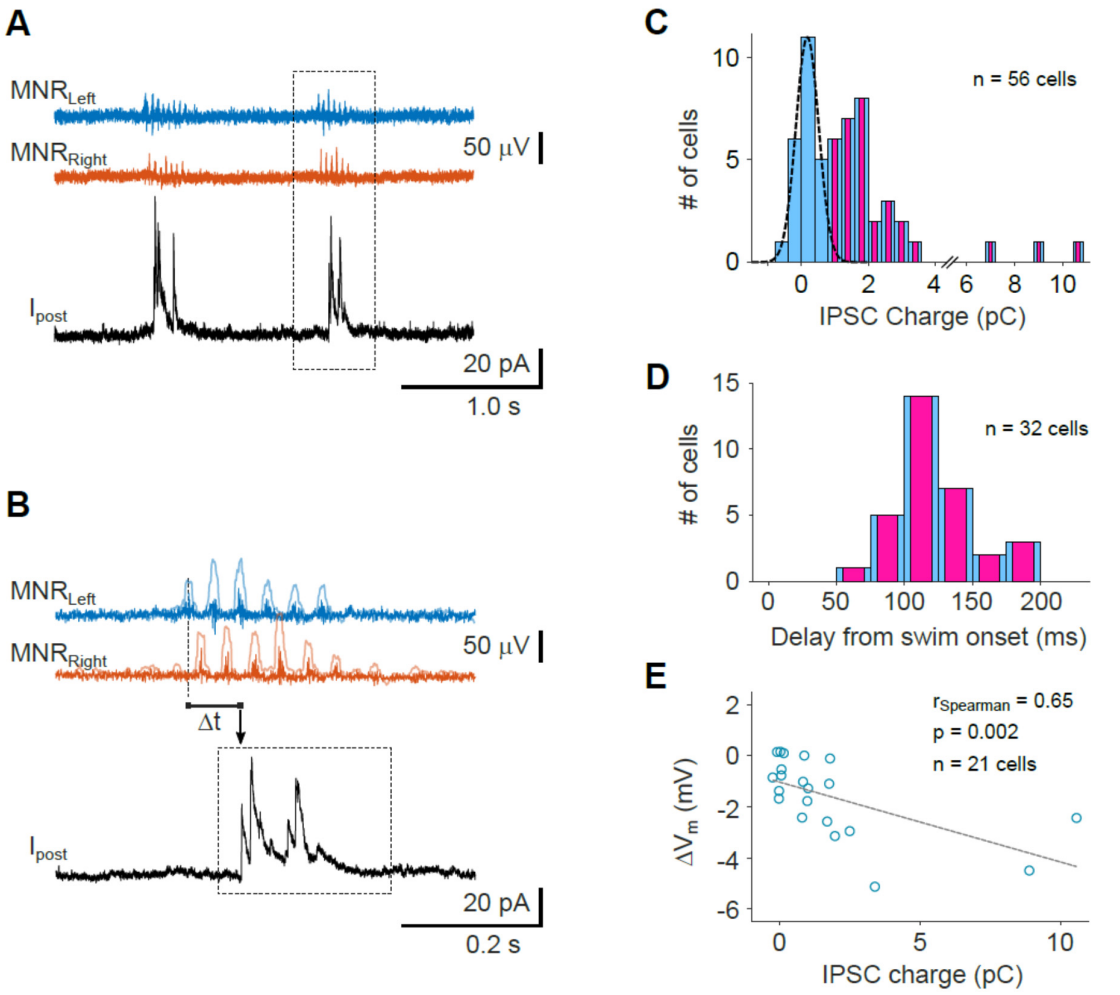

Figure 2. During spontaneous swim bouts, tectal neurons receive motor-related phasic inhibition

(A) Example recording of inhibitory membrane currents (I_{post}) during spontaneous fictive swim activity. Swim events (bursts in the MNR_{Left} and MNR_{Right} traces) are closely followed by short-lasting, large inhibitory postsynaptic currents (IPSCs) in a tectal neuron. Holding potential was +10 mV.

(B) Magnified view of the second event from (A). IPSC charge was measured in a 250 ms window (dotted rectangle). Delay (Δt) was measured between the first burst in the swim bout and the IPSC onset. MNR traces are overlaid with traces representing their standard deviation (see Methods).

(C) Histogram of inhibitory charge transfer in tectal neurons associated with spontaneous swimming (individual cell averages from n = 56 neurons). Dashed curve: Gaussian fit to the left peak of the charge histogram. In the majority of cells (n = 32), inhibitory charge transfer was larger 0.8 pC (bars co-labeled in magenta), indicating non-negligible inhibitory swim-related input.

(D) Histogram of delays between swim onset and IPSC onset. Individual cell averages from n = 32 cells with non-negligible inhibitory swim-related input.

(E) Scatter plot of swim-related transient hyperpolarization measured in current clamp (ΔV_m) and IPSC charge transfer measured in voltage clamp from a subset of cells in (C) where both modes of recording were applied (n = 21; 8 cells with IPSC charge <0.8 pC, 13 cells with charge >0.8 pC).

Fast inhibitory currents in tectal cells also occur during visually driven, directed swimming

Next, we investigated the extent to which motor-related CD signals also occur during visually evoked fictive swimming behavior. To do so, we combined single-cell patch clamp recordings with measurements of bilateral motor activity while presenting the larva with different visual stimulus patterns (Figure 3A). Previous work showed that both freely swimming and tethered larvae perform target-directed approach swims in response to small moving stimuli whereas large moving objects or expanding discs preferentially evoke escape swims[20,21,32,33]. Here we observed that also in the fictive swim preparation, larvae generated corresponding swim patterns when presented with these stimulus types. Notably, visually evoked swims were also accompanied by brief inhibitory synaptic currents, similar to those occurring during spontaneous swims (Fig. 3B). To elucidate whether larvae in the fictive swim preparation exhibited regular goal-directed swimming behavior, we used the bilaterally measured motor nerve activity to calculate the summed swim power and a direction index for each swim, as a proxy for the intended swim direction (Fig. 3C). This analysis showed that swims evoked by escape-inducing stimuli (large objects, looming discs), elicited swims with larger swim power than those occurring spontaneously or evoked by small moving objects (Fig. 3D). Importantly, swims evoked by small prey-like stimuli had a positive direction index, indicating appetitive, target-directed swimming, whereas those swims evoked by large or looming stimuli had negative direction indices. This strongly supports the notion that larvae in the fictive swim preparation exhibit normal swimming behavior, which much resembles that of freely or tethered larvae.

Next, we determined the synaptic charge transfer and delays of IPSCs for the different stimulus categories. For loom-generated escape swims, we observed a synaptic charge transfer significantly larger than that in the other stimulus categories (Fig. 3F), reflecting the higher swim power during loom-evoked escape swims (Fig. 3D). The IPSC delays did not differ significantly for different stimulus classes (Fig. 3G). Overall, the timing of the motor-related CD signal was relatively invariant. To test whether the strength of the inhibitory input correlated in any way with the motor activity measured on either side of the tail, we performed a multi-regression analysis of IPSC charge with measured unilateral swim power (Fig. 3H). This analysis showed that charge transfer (measured in tectal cells contralateral to the stimulated eye) was positively correlated

with swim power on the same side of the tail, contralateral to the stimulus (Figure 3H). In summary, we conclude that generally, any swim activity is accompanied by short inhibitory CD-like signals in the tectum and that the strength of this CD signal is positively correlated with the recruitment of muscular activity on the same side.

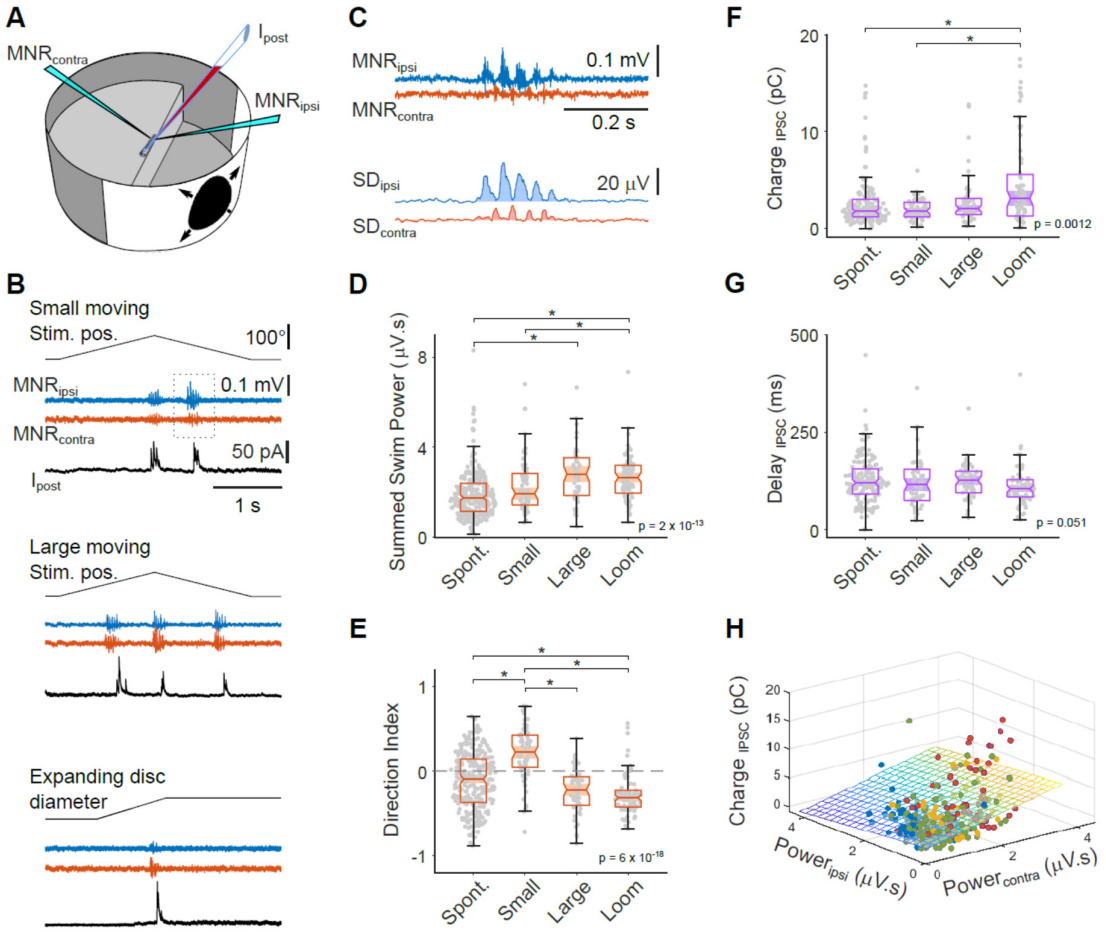

Figure 3. Fast inhibitory currents in tectal cells also occur during visually driven, directed swimming
(A) Recording configuration. Visual stimuli, here an expanding disc (looming stimulus), are projected on the side wall of the cylindrical arena.
(B) Simultaneous bilateral recording of motor nerve activity ($MNR_{ipsi,contra}$) and patch clamp recording from a postsynaptic tectal cell (I_{post}). Swim bouts are associated with transient inhibitory currents for swims of different directions (top, small horizontally moving rectangle; center, large horizontally moving rectangle; bottom, expanding disc). All traces from the same neuron.
(C) Magnified view of motor nerve recording (during small dot stimulation in (B), second swim bout) exhibits stronger activity on the side ipsilateral to the stimulus, indicating a swim directed at the target. Lower traces: standard deviation of motor nerve recording (10 ms moving window). Shaded areas indicate swim power on the ipsi- (blue) and contralateral (red) side.
(D) Sum of ipsi- and contralateral swim power for spontaneous and visually evoked swims (n = 493 bouts from 56 larvae). Swims in response to large dots and looms are stronger than spontaneous swims.

(E) Directional indices of spontaneous and visually evoked swims exhibit significant differences consistent with stimulus type (small object: target-directed; large object and looming stimulus: away from target). Same data as in (D).
(F) Inhibitory charge transfer associated with spontaneous and visually evoked swims. Data from recordings of cells with non-negligible charge transfer (>0.8 pC, magenta cells in Fig. 2C; 345 events from 32 cells).
(G) Delays between swim onset and IPSC onset for spontaneous and visually evoked swims exhibit no significant differences. Statistical differences between groups in panels D – G were evaluated using Kruskal-Wallis tests with Tukey-Kramer method for multiple comparisons.
(H) Scatter plot of IPSC charge transfer associated with spontaneous swims (green) and swims evoked by small dots (blue), large dots (yellow) and expanding discs (red). Colored plane indicates multiple regression model of charge transfer as a function of swim power in the ipsi- and contralateral motor nerve recording ($R^2 = 0.11$; *F*-value = 20.6; $p = 3.5 \times 10^{-9}$). Regression coefficient for swim power on the contralateral side is significantly different from 0 ($p = 4.4 \times 10^{-10}$), which is the side where the recorded tectal neuron is located, but not for ipsilateral swim power ($p = 0.07$).

Swim-related inhibition suppresses visually evoked spike output

If the CD signals observed here serve to suppress the processing of reafferent input that results from self-generated movement, then we expect to see an effect on visually evoked spiking activity. To test this, we used expanding discs as a stimulus because they elicited a transient increase in firing rate in many tectal neurons (Fig. 4A,B). We observed both an increase of the spike count, summed across the population of recorded cells (Fig. 4B), and depolarization of the membrane potential (after spikes were digitally removed; Fig. 4C) during looming stimuli. In addition, the looming disk stimuli evoked fictive escape swims (Fig. 4D).

Notably, in many cells, the firing rate was briefly reduced during a fictive swim burst or began to rise only afterward (Fig. 4Ai and ii). In other cells, swimming activity did not appear to affect firing rate (Fig. 4Aiii). To further address this, we determined the influence of swimming activity on firing rate by aligning looming-evoked firing rate changes relative to the swim onset (Fig. 4E). The time course of the firing rate relative to swim onset was variable for different cells (Fig. 4E): some cells started to fire before or during the swim bout, others started only afterwards. However, when aligned to the swim, the spike count summed over all cells showed a clear drop immediately after swim onset (Fig. 4F). The effect of motor activity on firing rate became clearer when we divided the data into two groups: those cells that received an appreciable inhibitory synaptic input during spontaneous swimming activity (a subset of 10 cells from those in Fig. 2C (magenta bars), with charge input >0.8 pC), and those that did not receive appreciable inhibitory input (a subset of 11 cells from those in Fig. 2C (blue bars) with IPSC charge <0.8 pC). The firing probability during a swim bout was strongly reduced in the group of synaptically inhibited cells (Figure 4G, magenta trace), whereas that in

the group without synaptic inhibition remained nearly constant (Figure 4G, blue trace). Moreover, the time course of the membrane potential (after removal of spikes) exhibited a significant, transient drop during swimming activity only in cells receiving synaptic inhibition, but not in those without inhibitory synaptic currents (Figure 4 H,I). Collectively, we found that an inhibitory CD signal briefly suppresses visually driven activity in many tectal cells, which suggests that a neuronal correlate of motor-related suppression, or 'saccadic suppression' in a broader sense, is implemented in the tectal circuitry.

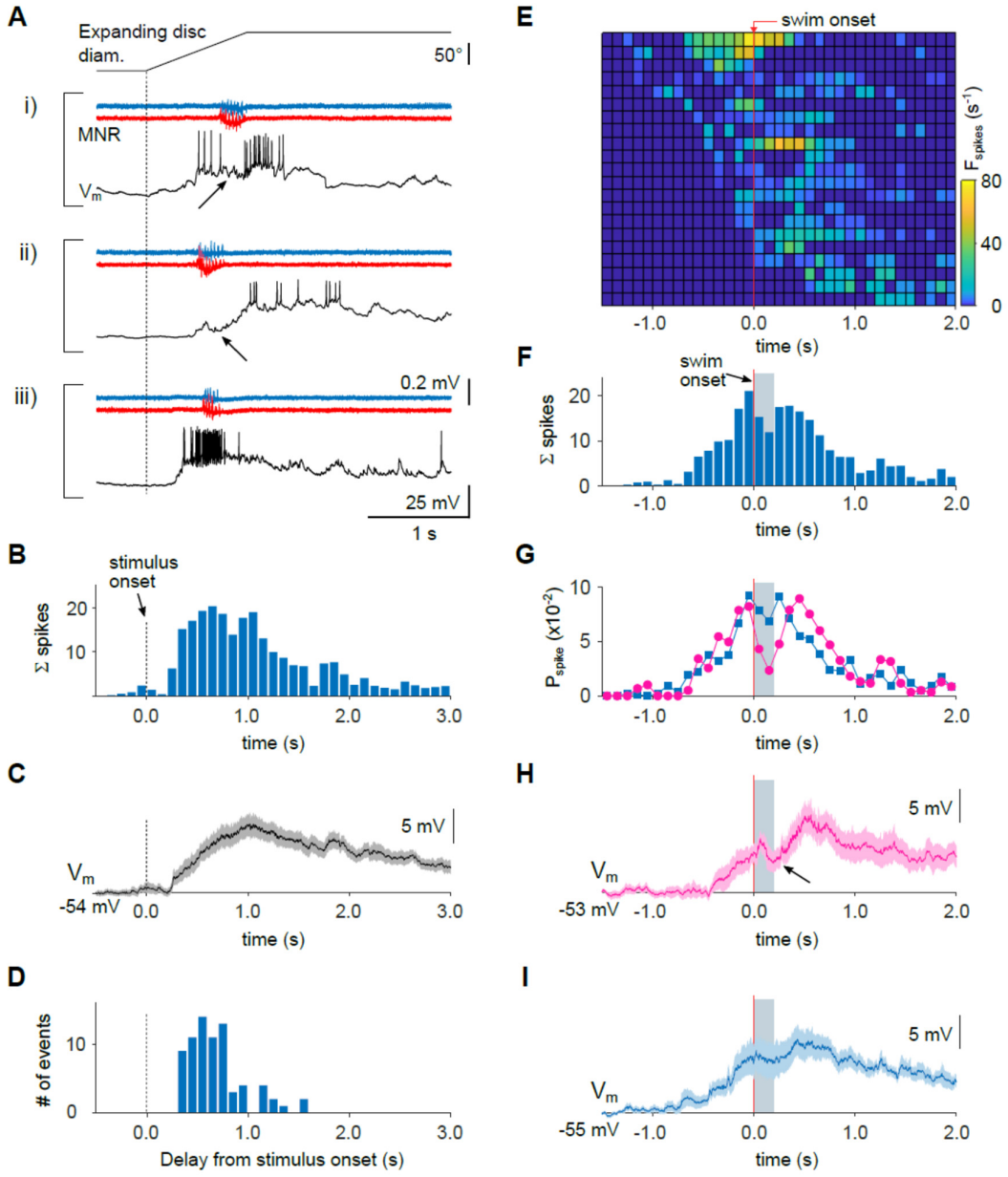

Figure 4

Figure 4. Swim-related inhibition transiently suppresses visually evoked spike output in tectal cells
(A) Three motor nerve recordings (MNR) of looming-evoked swim events and simultaneously recorded spiking activity in three tectal neurons (V_m). Swim events are often associated with a reduction in cell spiking (arrow in i), or a transient decrease in membrane voltage (arrow in ii), while other cells did not show a noticeable change (iii). Stimulus onset indicated by vertical dashed line.
(B) Population spike time histogram, evoked by looming stimuli. Spikes were counted in 100 ms bins, averaged across sweeps for each cell and then summed over all cells (n = 21).
(C) Membrane voltage change of the recorded cells in response to looming stimuli. Average across individual, baseline-subtracted cell averages (n = 21 cells, mean ± SEM). Spikes digitally removed.
(D) Delay histogram of fictive swim events relative to stimulus onset.
(E) Histogram of instantaneous spike rate, evoked by looming disc stimuli, aligned to swim onset. Each row represents recording from one cell (n = 21). Spikes were counted in 100 ms bins and averaged across sweeps for each cell. Rows in histogram vertically sorted according to onset of cell spiking relative to swim onset.
(F) Population spike time histogram, aligned to swim onset (vertical red line), summed over all cells shown in (E).
(G) Time course of the spike probability aligned to swim onset, for cells with detectable inhibitory synaptic charge transfer (magenta) and negligible charge transfer (blue), respectively. Note the strong transient reduction in spike probability in a ~200 ms window in the magenta trace, coinciding with the swim event (grey bar).
(H,I) Membrane voltage traces (spikes digitally removed), aligned to swim onset. Note the transient decrease in membrane voltage during swimming (arrow in H) for cells with inhibitory charge transfer >0.8 pC (panel H, magenta. Average drop in V_m = -2.8 ± 0.9 mV, n = 10 cells, p = 0.014, Wilcoxon signed-rank test), but not in cells with negligible charge transfer <0.8 pC (panel I, blue. Average drop in V_m = -0.6 ± 0.9 mV, n = 11 cells, p = 0.7). Traces show averages across individual, baseline-subtracted cell averages (mean ± SEM, n = 10 cells in H, n = 11 cells in I).

Swim-related inhibitory CD signals are timed to cancel excitatory inputs evoked by fast whole-field motion stimuli

If the CD signals observed here serve to specifically suppress those excitatory signals in the tectum that arise from the abrupt shift of the retinal image during a swim bout (reafference), then this excitation and the inhibitory CD signal must coincide in time. To test this, we measured the time course of excitatory postsynaptic currents evoked by a wide-field motion stimulus, as would be expected during an abrupt, discrete movement (Fig. 5A). During forward swimming, optic flow sweeps across the retina in the front-to-back direction. We observed that a grating moving abruptly from front-to-back evoked phasic excitatory currents in tectal neurons. The delay between movement onset of the stimulus and the excitatory current was 155 ms ± 10 ms (mean ± SEM, n = 17 cells). This is comparable with the latencies of about 75 - 150 ms measured for inhibitory CD signals (Figure 2D). We conclude that the motor-related CD signal is appropriately timed to shunt self-motion-generated excitation in the tectum.

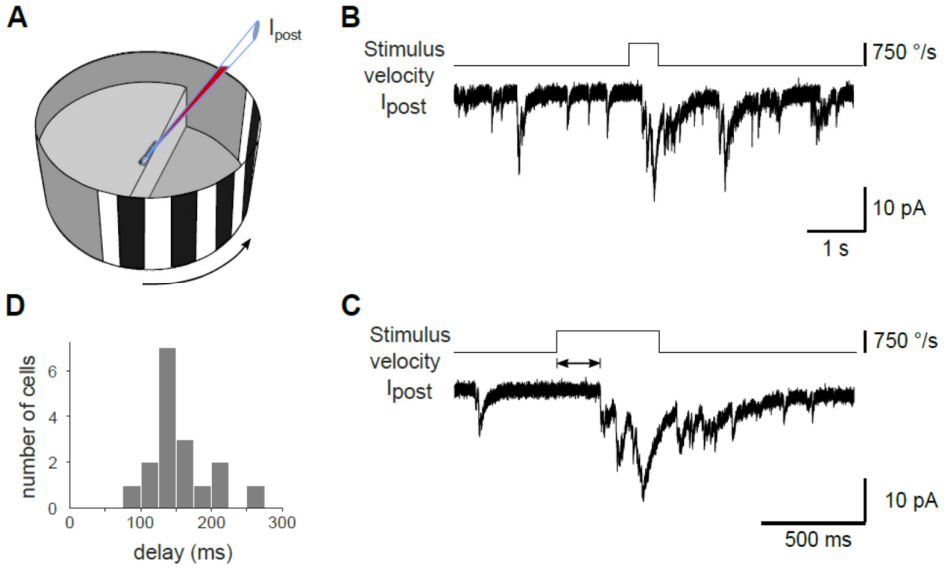

Figure 5. Latency of excitatory input evoked by fast whole-field motion stimuli
(A) Experimental configuration. Excitatory currents were recorded in voltage clamp (holding potential -60 mV) from cell contralateral to the stimulus. A stationary grating was shown, which abruptly moved backward, simulating reafferent whole-field visual motion during discrete swim bouts.
(B) Example recording of EPSCs (I_{post}) during presentation of grating, which moved rapidly for 0.5 s (upper trace).
(C) Magnified view of the postsynaptic current shown in (B).
(D) Histogram of delays between stimulus onset and EPSC onset. Individual cell averages from n = 17 cells (155 ms ± 10 ms; mean ± SEM).

Spatial distribution of swim-related Ca2+ signals in the tectal neuropil

Next, we searched for evidence where in the tectal neuropil the phasic inhibitory CD signal may be transmitted. As feature- and task-related synaptic inputs are often localized in specific tectal layers[25,34], we examined whether there is evidence for a laminar organization of swim-related CD signals. We argued that presynaptic compartments that phasically release an inhibitory transmitter shortly after swim onset should exhibit a transient increase in [Ca2+], whose rising phase represents the time of presynaptic action potential firing[35] and should hence start only after the swim onset (Fig. 6A). We therefore used two-photon Ca2+ imaging at high spatial and temporal resolution in a transgenic line that expresses GCaMP5G pan-neuronally[36] and characterized in a central strip of the neuropil the distribution of Ca2+ transients that occurred around the onset of spontaneous swim bouts (Figure 6A-C). We systematically subdivided the imaged area into small ROIs (Fig. 6C) and determined

the onset of Ca2+ transients in a time interval ±2.0 seconds from the onset of a spontaneous swim bout. We found that Ca2+ transients occurred throughout the neuropil, starting before or after the onset of swimming (Figure 6C). The occurrence of Ca2+ transients rose within ~500 ms before swim onset (Fig. 6D), consistent with the idea that spontaneous tectal activity contributes to the triggering of spontaneous swimming[37]. Notably, however, 13% of all Ca2+ transients began in a time window 50 to 250 ms after swim onset (Fig. 6D). We hypothesize that these post-swim Ca2+ signals reflect at least in part activity in those presynaptic compartments that transmit the inhibitory CD signal. Therefore, we examined how active ROIs (corresponding to those, where a Ca2+ transient was detected) were distributed in time and space across the neuropil (Figure 6E). The distribution was remarkably non-uniform: active ROIs were clustered around the time of swim onset in the deep neuropil (depth level 0-20%, containing the SAC), and in the most superficial layer (depth level 90-100%, containing SM and SO). In the SAC, in which also the proximal axons of tectal projection neurons are packed, the number of active ROIs peaked in the interval [-50; +50 ms], around the onset of swimming, consistent with the notion that tectal premotor activity is transmitted via this pathway and contributes to triggering a spontaneous swim. Most notably, however, in the SM/SO relatively little activity occurred before swim onset. Instead, the number of active ROIs peaked in the interval [+50; +150 ms] after swim onset, and dropped rapidly thereafter. The cumulative frequency histogram of Ca2+ transients in an interval of ±500 ms, pooled according to the stratification of the tectal neuropil, showed that Ca2+ signals in the superficial SM/SO and the deep SAC peaked around swim onset, whereas those in the more central layers containing the SFGS and SGC were more uniformly distributed (Fig. 6F). We compared the fraction of Ca2+ transients starting at or later than 50 ms after swim onset ('post-swim') for each of these neuropil regions to that across all layers (Fig. 6G). Notably, in the SM/SO layer, Ca2+ transients occurred significantly more often in the post-swim interval compared to the distribution across all layers. Most types of tectal neurons do not extend neurites in this very superficial neuropil region. Instead, it is strongly innervated by afferent fibers from the mediodorsal torus longitudinalis (TL)[38,39] (see Discussion). Together, as the timing of Ca2+ transients in the SM/SO agrees well with the timing of the synaptic CD signal, we conclude that the most superficial neuropil is a key input layer for CD signals arriving from extratectal sources.

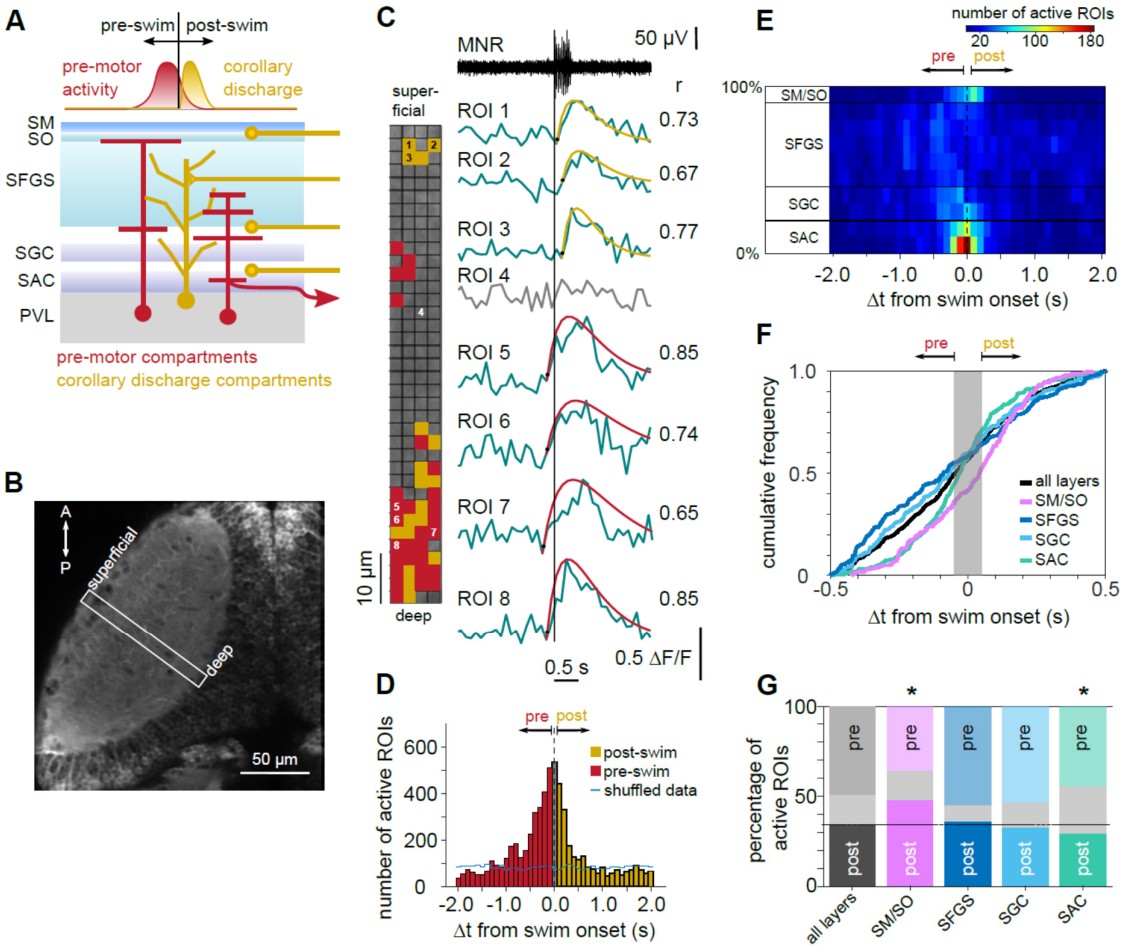

Figure 6. Spatial distribution of swim-related Ca2+ signals in the tectal neuropil

(A) Schematic of tectal layers, showing interneurons, projection neurons and incoming axons that could potentially mediate pre-motor (red) or corollary discharge activity (gold), respectively.

(B) Tectal hemisphere in *Tg(elavl3:GCaMP5G)*, dorsal view. Rapid Ca2+ imaging was performed in a rectangular scan area (white box) covering deep to superficial neuropil during spontaneous fictive swims.

(C) Example of fluorescence transients (green traces) from small regions-of-interest (ROIs) in the neuropil around swim onset (vertical line). Swim onset was determined from simultaneous motor nerve recording (MNR, top). Fluorescence traces 1-8 taken from ROIs marked by numbers in the left inset. Inset shows the scanned region divided into a grid of ROIs. Fluorescence trace from each ROI was fitted with a Ca2+ response function (smooth curves, see Methods). ROIs were considered 'active' if the correlation coefficient of the raw trace with its model fit (indicated on the right) exceeded a threshold of 0.65. Other ROIs were considered inactive (compare ROI 4). The onset of Ca2+ transients (black circles) in active ROIs was used to determine the time of lead or lag relative to swim onset. Colored regions in inset mark active ROIs, categorized according to whether their onset was pre-swim (red) or post-swim (gold).

(D) Histogram of active ROI onsets. Data from 315 spontaneous swims in 15 larvae; total of 6042 active ROIs. Active ROIs cluster around the time of swim onset. Blue line indicates control distribution of active ROIs when fluorescence data was circularly shuffled before alignment with motor nerve recording.

(E) Space-time histogram of active ROIs. Active ROIs from (D) were binned according to their location in the neuropil. Spatial bin size is 10%, where deep neuropil boundary corresponds to 0% and the superficial boundary to 100%. Spatial bins are grouped according to anatomical layers: 0-20%, containing *stratum albium centrale* (SAC); 20-40%, containing *stratum griseum centrale* (SGC); 40-90%, containing *stratum fibrosum et griseum superficiale* (SFGS); 90-100%, containing *stratum marginale* and *stratum opticum* (SM/SO). Note that most peri-swim active ROIs within a ±250 ms window are located in SAC and SM/SO, with the latter containing mainly post-swim active ROIs.

(F) Cumulative frequencies of active ROIs, pooled over all layers (black trace) and pooled separately for the different neuropil regions indicated in panel (E). Active ROIs with onset times <-50 ms are considered 'pre-swim', those with onset times >+50 ms 'post-swim'. Active ROIs with onset in the central bin [-50; +50 ms] (grey bar) are not categorized because of uncertainty about their exact onset relative to swim onset. Note the steep rise of SAC- and SM/SO-curves in the range from -250 ms to +250 ms, but not SGC and SFGS.
(G) Fractions of active ROIs from the ±500 ms peri-swim interval in (F) classified as 'pre-swim' vs. 'post-swim' pooled over all layers (left bar) and pooled separately for the different neuropil regions. In the superficial SM/SO layer, Ca2+ transients occurred more frequently in the post-swim interval ($p = 2.3 \times 10^{-7}$) compared to the distribution across all layers. In the SAC layer, Ca2+ transients occurred less frequently in the post-swim interval ($p = 1.1 \times 10^{-3}$; binomial tests with Bonferoni correction for multiple comparisons). Central grey regions in each bar represent events in the central bin [-50; +50 ms], not included in pre-swim vs post-swim categorization.

Cells with diverse dendritic morphologies receive CD synaptic inhibition

We further searched for cues where in the tectal neuropil inhibitory CD signals may be transmitted. If CD signals enter the tectum in the SM/SO layer, do only those cells that extend dendrites all the way up into the most superficial neuropil receive motor-related inhibitory synaptic input? We examined this by comparing the dendritic profiles of recorded neurons with and without CD synaptic inhibition (Fig. 7A-D). GFP-positive cells recorded in the *Tg(pou4f1-hsp70l:GFP)* line had many neurites extending in the deep neuropil (Fig. 7A,B). They did not, however, arborize in layers more superficial than the central SFGS, making it unlikely that they receive direct synaptic input from a CD-mediating afferent input in the SM/SO. Also, whether or not a cell received motor-related inhibition was unrelated to its dendritic profile (compare Fig. 7B, upper vs. lower panel). Interestingly, GFP-positive cells, which represent to a large part projection neurons[31], were not the only cells receiving CD inhibitory input. When patching GFP-negative neurons, we observed cells with markedly distinct morphology also receiving phasic motor-related inhibition (Fig. 7C,D). For example also cells appearing to be local interneurons, such as bistratified neurons with a dorsal dendritic branch near the SFGS/SO boundary, were among those with CD inhibitory input. Together, the finding that cells without dendrites any near the superficial SM/SO still receive strong motor-related inhibition suggests that there is a type of inhibitory relay neuron in the tectum that converts an excitatory CD input into a local inhibitory signal and distributes it across one or more layers.

To further corroborate this, we investigated the distribution of inhibitory synapses in the neuropil. As fast inhibitory transmission in the teleost tectum is predominantly mediated by $GABA_A$ receptor channels, we used antibody labeling against the GABAR

subunits β2/β3, which are strongly expressed in the tectal neuropil and localize in specific layers in several adult teleost species[40-42]. We argued that laminae in the neuropil that lack $GABA_A$ receptors could be excluded as layers in which strong inhibitory CD signals are transmitted. Contrary to that notion, we observed immunoreactivity against GABAR subunits β2/β3 across all layers, without a distinct laminar organization (Fig. 7E-G). Furthermore, GABAR β2/β3-subunits were also detected within the periventricular cell body layer (Fig. 7H). The diffuse distribution of GABA receptors suggests that the transmission of inhibitory CD signals need not be restricted to one or a few specific layers but can in principle reach a variety of morphologically distinct tectal neurons in different layers of the neuropil.

Together, these observations suggest that motor-related inhibitory signals are distributed widely across the tectum, exerting a transient suppressive effect on multiple cell types with distinct functional roles.

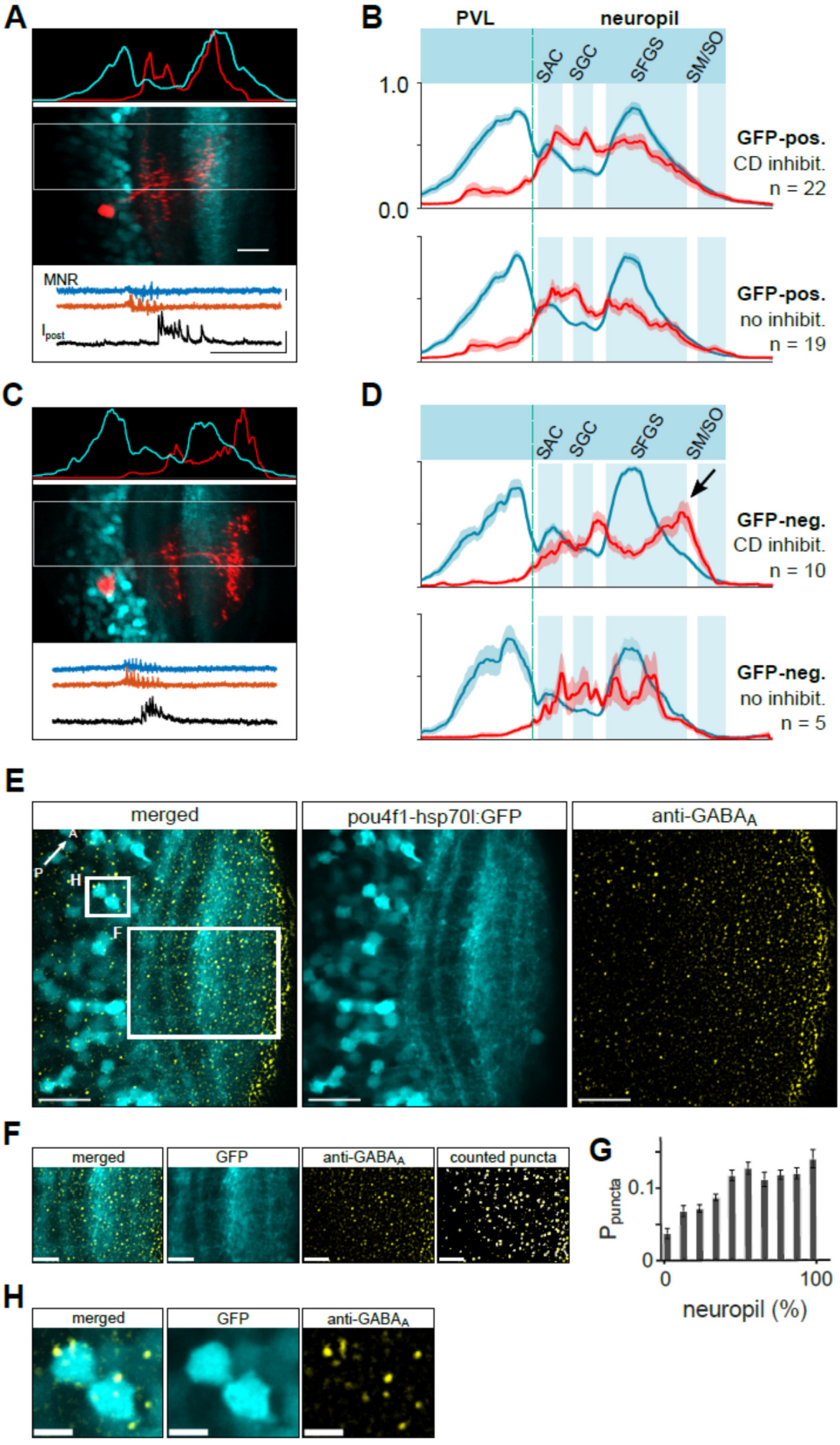

Figure 7

Figure 7. Dendritic profiles of tectal cells with CD synaptic inhibition and distribution of GABA receptor subunits

(A) Dendritic profile of a recorded GFP-positive neuron labeled with sulforhodamine (red) in the *Tg(pou4f1-hsp70l:GFP)* line (cyan). Scale bar 20 μm. Profiles of fluorescence intensity (top inset, peak-scaled) were measured separately in the red and cyan channel of the dual color image (center) across the PVL and neuropil (rectangular area in center image). The recorded neuron received CD inhibitory postsynaptic currents associated with swimming (bottom inset). Scale bars MNR: 50 μV, I_{post} 50 pA, time: 500 ms).

(B) Average dendritic profiles of recorded GFP-positive neurons, for cells with motor-related, CD inhibition (top) and without CD inhibition (bottom). Profiles were aligned with respect to the PVL/neuropil boundary and the peak of the SFGS and averaged (cyan traces, mean ± SEM). Profiles of neurons (red) exhibit dendrites mostly in SAC, SGC and central SFGS, but not in more superficial layers.

(C) Same as in (A), but for a GFP-negative neuron patched in the *Tg(pou4f1-hsp70l:GFP)* line. Note the bistratified dendritic profile, with the upper dendrites in target layers more dorsal to those of GFP-positive neurons.

(D) Same as in (B), but for GFP-negative neurons patched in the *Tg(pou4f1-hsp70l:GFP)* line. Note the peak of dendritic profiles superficial to the SFGS (arrow).

(E) Single optical section of GFP fluorescence and immunostaining of a tectal hemisphere in a 5 dpf larva (dorsal view). *Middle*: GFP expression in *Tg(pou4f1-hsp70l:GFP)*. *Right*: anti-$GABA_A$ receptor immunostaining. *Left*: merged image of both channels. Scale bar 20 μm.

(F) Neuropil region indicated by large box in (E) showing the merged (left), the GFP-stratification pattern in the neuropil (middle left), and localization of $GABA_A$-positive puncta (middle right) in the neuropil. Puncta exceeding thresholds for size and circularity (marked with a white outline in rightmost panel) were counted as $GABA_A$ receptor clusters representing putative inhibitory synapses and included in the histogram (G). Scale bar 10 μm.

(G) Histogram of relative abundance of $GABA_A$-positive puncta in the tectal neuropil as a function of neuropil depth (mean ± SEM; n = 11 samples). 0% corresponds to PVL/neuropil boundary, 100% to dorsal neuropil boundary, bin width 10%.

(H) Magnified view of region indicated by box in (E) showing the merged (left), the GFP expression (middle), and $GABA_A$–positive puncta (right). Note colocalization of $GABA_A$ receptor-positive puncta and surface of GFP-positive cell bodies. Scale bar 5 μm.

DISCUSSION

We discovered a robust synaptic CD signal in visually driven neurons of the optic tectum. We observed this phasic inhibitory input, which was temporally locked to fictive motor activity, in many cells with different morphologies, both during spontaneous and visually evoked swim patterns. Strikingly, this inhibitory input suppressed action potential firing during discrete fictive swim bouts, supporting the notion that the processing of sensory activity arising from self-motion (reafference) is effectively suppressed at the level of the optic tectum. Ca2+ imaging in the tectal neuropil revealed an unexpected clustering of post-swim Ca2+ signals in the most superficial layer, suggesting that CD signals may enter the tectum in this layer from an extratectal source (Fig. 8). The results are significant as they suggest a new model for investigating saccadic suppression, tractable at the cellular and synaptic level, in the retino-tectal pathway.

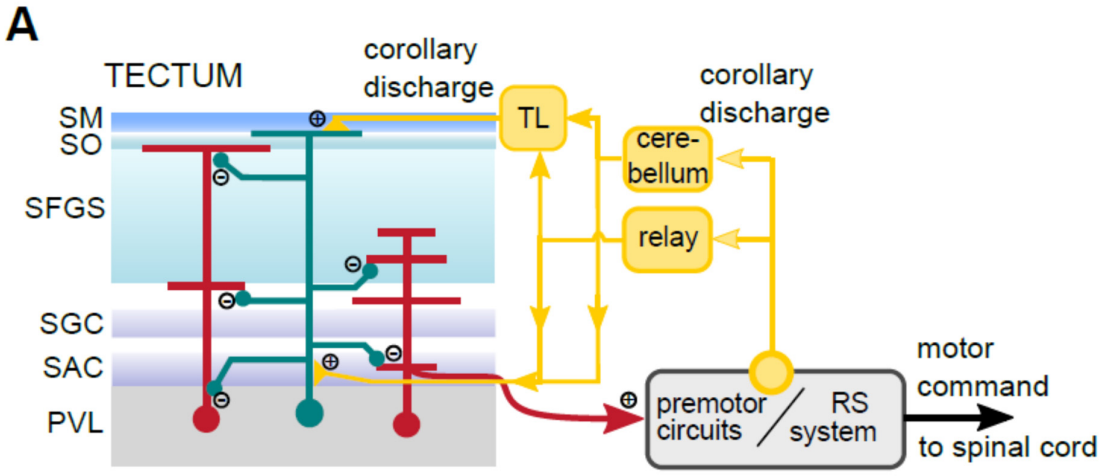

Figure 8. Putative mechanism of CD signaling in the visuomotor pathway

(A) Hypothesized organization of inhibitory CD signaling in the tectum. Diverse cell types in the tectum (red cells) receive motor-related inhibitory inputs during swimming. The CD signal is initiated at unknown sites in premotor circuitry controlling tail and eye movements (yellow circle) and is relayed to the tectum, possibly via the cerebellum or another relay node. Because post-swim Ca2+ signals cluster in the most superficial layer containing the stratum marginale (SM) where axons from TL projection neurons form a narrow input layer, TL is a likely pathway by which CD signals reach the tectum. Similarly, afferents from the cerebellum, which preferentially terminate in deep neuropil layers containing the SAC, could form another input channel for CD signals. Because projection neurons from both the TL and the cerebellum are mainly glutamatergic, this model posits that the afferent CD signal is sign-converted by local inhibitory interneurons (green). In the case that CD is relayed by superficial TL fibers, this interneuron type is expected to receive excitatory input in the SM/SO layer and distribute inhibitory signals across several neuropil layers. This could explain how also neurons with only deep dendritic branches receive phasic inhibitory inputs despite a lack of dendrites in the more superficial layers (red neuron on the right).

Functional role of the inhibitory CD signal in tectal circuitry

Generally, CD signals inform sensory brain areas about ongoing self-generated movements and influence the processing of incoming sensory signals. In what way does the CD signal discovered here influence ongoing visuomotor processing?

Apparently, the CD inhibitory input is effective in suppressing tectal output activity in the moment the larva swims in a saccade-like manner. This is because first we observed that in the *Tg(pou4f1-hsp70l:GFP)* line, GFP-positive neurons, whose axons contribute to a distinct output channel projecting from the tectum to hindbrain premotor circuits[31], received a pronounced motor-related inhibitory input (Fig. 2) and exhibited transient suppression of spiking (Fig. 4). Second, the inhibitory CD signal was adequately timed to coincide with, and therefore counteract, the reafferent excitation evoked by global stimulation of the retina, expected to arise from the fish's own locomotion (Fig. 5). Third, since the CD signal was robust and its timing relatively independent of the duration, direction, and strength of the fictive swim bout (Fig. 3), this suggests that it has a suppressive effect on tectal output signals during all types of swims.

In other systems, CD signals have been found to encode a “negative image” of the reafferent sensory input due to the animal’s self-motion, which is then subtracted from the actual afferent input[4,14,43]. We observed that the inhibitory charge transfer was correlated with swim power measured on the same side (Fig. 3). This suggests that in addition to its role of attenuating tectal output, the observed CD signal could encode quantitative information on the expected reafferent visual input during different swim patterns, e.g. when turning in one or the other direction in response to appetitive and aversive stimuli[20,21], or at different swim speeds[44]. Thus, the CD signal observed here could in principle be more than a simple signal for saccadic suppression, but may be a component of a predictive signal, distributed across many cell types in visual areas, that represents an ‘internal model’ of the expected visual input during swimming[45]. In that case, a mismatch between the CD internal model and the actual reafferent input would serve as an error signal that instructs motor learning on slower time scales[28]. Such error signals could be critical in modifying synaptic weights between visual and motor areas in order to adapt the visuomotor transformation to a change in external or

internal conditions, such as changes in the surrounding medium, or changes in the skeletomuscular apparatus as the animal grows.

Finally, a transient inhibitory input may also have a facilitating effect[6,46] and sensitize the visual circuitry for subsequent detection of behaviorally relevant, local stimuli, such as prey-like objects. This is because a synchronous, widely distributed inhibitory input will counteract the expected widespread depolarization of tectal cells from the wave of self-motion induced retinal inputs, remove depolarization block after the phasic inhibitory inputs have decayed, and may lower the threshold for generating subsequent, target-directed premotor activity[37,47]. When performing motor sequences to capture prey, zebrafish larvae exhibit reduced reaction times when the stimulus reappears immediately after a previous swim bout has ended[21]. This behavioral effect could be explained if the stimulus-evoked, retinotopically organized input arrives on a sensitized tectal circuitry, in which activity from previous stimuli and self-motion induced optic flow has been quenched by a global inhibitory signal. Furthermore, since the inhibitory CD signal effectively forms a negative feedback loop, this system could be prone to oscillatory behavior and contribute to setting the inter-bout interval of swim sequences.

Collectively, the CD signal could serve multiple roles in that (1) it blocks or attenuates tectal output to hindbrain premotor circuits at the time of swimming; (2) it could be the basis for computing an error signal relevant for motor learning if the expected and the actual visual feedback do not match; and (3) it could render tectal circuits more sensitive immediately after a discrete swim bout for accelerated detection of local stimuli and faster behavioral performance. The zebrafish model offers opportunities to test these possibilities in the future. Furthermore, zebrafish also exhibit robust optokinetic responses that depend on neuronal populations in the pretectum[48]. It is of interest whether also neurons in the pretectal visual pathway receive an inhibitory CD signal, which may be addressed in future experiments.

Possible sources of CD signals and circuit mechanism

The pathway that evokes the phasic, motor-related inhibitory signal in the tectum must be activated by premotor neural circuitry whose activity triggers the recruitment of motor neurons in the spinal cord. The origin of the CD pathway, from where motor-

related signals are sent towards sensory areas is unclear, but we can go backwards and ask by which route motor-related CD signals enter the tectum. Apart from retinal inputs, the tectum receives afferent fibers from several non-sensory areas. Tectal afferents have been described in the larva whose cell bodies are located in the nucleus isthmi in the tegmentum[49,50], the thalamus[51], rostral hypothalamus[52], the raphe nucleus[53,54], pretectum[55,56], the cerebellum[57], and the torus longitudinalis[39]. Most of these regions are unlikely to relay a CD signal to the tectum because they are mainly visually responsive (thalamus, nucleus isthmi)[49-51], or exert state-dependent modulatory influence on tectal processing on slower time scales (hypothalamus, raphe nucleus)[52-54].

By contrast, evidence for the torus longitudinalis as a mediator of motor-related CD signals in the tectum comes from our Ca2+ imaging experiments, which showed that transient post-swim activity, whose timing is consistent with that of the motor-related inhibitory synaptic input, clustered in compartments in the dorsal SM/SO. It is this layer, where the axons from TL projection neurons form the only source of afferent input and synapse on tectal neurons[39]. Furthermore, some TL neurons in several ray-finned fish species exhibit transient activity during saccadic eye movements[38]. Together, this makes TL projection neurons one of the likely candidates as relays for the inhibitory CD signal found in our recordings. The afferent pathways that drive CD activity in TL projection neurons are unclear, but potential sources are cerebellar projection neurons and cells near the cerebellar valvula[38,57,58].

Also, motor-related output from eurydendroid projection neurons[59,60] in the cerebellum is another potential source for CD signals in the tectum. First, axons from some eurydendroid cells densely and extensively innervate deep layers of the tectal neuropil[57]. Second, the activity of eurydendroid cells is correlated with both spontaneous and evoked motor events[61]. The coincidence of eurydendroid activity with swimming is not surprising because their presynaptic excitatory inputs, the parallel fibers of cerebellar granule cells[59,60], also exhibit markedly increased firing rates during brief swim bursts[62]. Therefore, cerebellar output may -- either directly or indirectly via the TL -- channel motor-related information into the tectal neuropil. It should be noted, however, that both cerebellar eurydendroid cells and most or all TL granule cells are glutamatergic[38,39,60], so this possible CD-pathway requires at least

one additional sign-converting relay neuron. Several types of inhibitory interneurons have been identified in the tectum that could serve this role [25,63].

In summary, the evidence from our data as well as previous studies on the anatomy and function of cerebellar projections favors a model of a feedback loop sending a CD signal from the pre-motor circuitry in the mid- and hindbrain, passing through the cerebellum and TL (and possibly other relay nodes) into the tectum (Fig. 8).

Implications for saccadic suppression in mammalian systems

In mammals, the emergence of thalamo-cortical visual circuits in addition to the evolutionarily conserved visual pathways in the brainstem provides for a fundamental extension of visual processing power. Nevertheless, or rather because of this, motor-related modulation is ubiquitous in cortical processing[45]. Indeed, evidence for perisaccadic modulation of neuronal activity during eye movements is well established in several cortical areas[11-13,64,65]. Here, CD signals are considered a critical factor underlying perceptual saccadic suppression and enhancement[3,46], which enables perceptual continuity during self-generated eye movements. It is of note that CD signals implicated in cortical processing are likely mediated by the midbrain superior colliculus[3,64], thus forming a functional bridge between subcortical and cortical visual processing. But more than just being the source of CD, superior colliculus neurons themselves are a target of motor-related modulation as their responses are altered during saccadic eye movements in cats[66] and primates[10,67], and also during locomotion in the rodent SC[68]. This is similar to the suppression of activity we observed in visually responsive interneurons as well as output neurons in the optic tectum that project to motor areas. In the mammalian superior colliculus, an intracollicular inhibitory circuit motif could in principle mediate CD-like inhibition in visual neurons in more superficial layers[69], but also purely retinal mechanisms could contribute to it[70]. The mammalian superior colliculus and its homologous region, the optic tectum in non-mammalian vertebrates, share fundamental properties[71,72]. Our results suggest that a temporally robust inhibitory synaptic input driven by an extratectal circuit mediates this suppression in the optic tectum in zebrafish during saccade-like locomotion. In the mammalian superior colliculus, recordings of saccade-related synaptic inputs may provide cues for potentially similar synaptic mechanisms.

METHODS

Zebrafish

Zebrafish larvae (*Danio rerio*) were raised at 28.5°C in embryo medium in a 14 h/10 h light/dark cycle. Experiments were performed on zebrafish larvae 5-8 days post-fertilization, before sexual differentiation. The following transgenic lines were used: For electrophysiological recordings and immunohistochemical analysis, *Tg(pou4f1-hsp70l:GFP)*[30,31], in which GFP is expressed in retinal ganglion cells and a subset of tectal periventricular neurons. For Ca2+ imaging, *Tg(elavl3:GCaMP5G)*[36] in the *nacre* background[73], in which the genetically encoded Ca2+ sensor GCaMP5G is expressed pan-neuronally[36,74]. All procedures were performed following the guidelines of the German animal welfare law and approved by local authorities (Regierungspräsidien Karlsruhe and Freiburg).

Electrophysiology and visual stimulation

Preparation and solutions: For electrophysiological recordings, zebrafish larvae were anesthetized using 0.02% MS-222 (tricaine methane-sulfonate, Sigma Aldrich) and then immobilized by incubation in α-bungarotoxin (1.0 mg/ml dissolved in embryo medium, Tocris). The larva was transferred to a custom-made cylindrical recording chamber (5.0 cm outer diameter, 2.5 cm height). It was mounted in an upright position at mid-height of the chamber on a Sylgard-shelf that covered 50% of the bottom to leave an unobstructed view for visual stimulation (see Fig. 3A). The chamber was filled with extracellular solution containing (in mM): NaCl (134), KCl (2.9), $CaCl_2$ (2.1), $MgCl_2$ (1.2), HEPES (10), and glucose (10), pH 7.8, 290 mmol/kg. To approach tectal cells for whole-cell recordings, a small opening was made in the skin above the optic tectum using an etched tungsten needle. The preparation was then moved to a custom-built two-photon laser scanning microscope equipped with infrared transmission optics to enable positioning of recording electrodes for electrophysiological experiments. Targeted patch clamp recordings of GFP-expressing cells were established using a water immersion objective (Zeiss 20x/1.0 NA) and two-photon laser excitation at 940 nm. Emission light was spectrally separated using two band pass filters (green: HQ 515/30 nm; red: HQ 610/75 nm, AHF, Germany).

Recordings: To record fictive motor activity, two suction electrodes (borosilicate glass pipettes with heat-polished tips; open tip diameter ~30 μm) were filled with extracellular solution and positioned on intersegmental boundaries in the midrange of the intact tail, one on each side, and gentle suction was applied[27]. Bilateral motor nerve activity was recorded in current clamp mode, low-pass filtered at 3 kHz. Once spontaneous motor nerve activity was detected, a whole-cell recording from a tectal cell was established under visual control using the two-photon fluorescence optics of the microscope by which fluorescence of GFP-labeled cells and the patch pipette containing sulforhodamine could be monitored in real time[29]. Patch pipettes were pulled from borosilicate glass and filled with intracellular solution containing (in mM): K-Gluconate (125), HEPES (10), EGTA (10), $MgCl_2$ (2.5), ATP-Na_2 (4), and GTP (0.3), Sulforhodamine-B (360 µM, Invitrogen), pH 7.3, 290 mmol/kg. Open tip resistance was 8-14 MΩ. In some recordings, K-Gluconate was replaced with Cs-Gluconate (120 mM) to minimize leak potassium currents during voltage clamp. Inhibitory synaptic currents were measured at a holding potential of 0 to 10 mV. Whole-cell current and voltage signals were recorded using a Multiclamp 700B amplifier, filtered at 3 kHz. The simultaneous bilateral motor nerve recordings and the single-cell patch clamp recording were sampled at 10 kHz on the same computer using a PCIe-6251 board and a custom-written script in LabView (National Instruments, USA).

Visual stimulation: Visual stimuli were projected on a diffusive screen (Ecolor#216, Rosco) attached to the side wall of the recording chamber, using a micro projector (Optoma PK102, or Kodak Luma 75). The projection area covered approx. 120° (azimuth) and 55° (elevation) of the visual field of the stimulated eye, without obstruction from the sylgard shelf or distortions from water-air interfaces (compare Fig. 3A). To evoke target-directed, prey tracking-like swims, a small white rectangle moved on a dark background (target size ≤6° height, ≤12° width)[21]. To evoke avoidance swims away from the target, a large white rectangle (≥12° height, ≥24° width) moved on a dark background or an expanding dark disc was shown on a white background ('looming object'). Moving targets appeared in the caudal visual field, moved forwards and then backwards at a speed of 70°/s, covering ~100° of the horizontal visual field (from -110° to -10°, where 0° refers to the heading direction of the larva). Expanding discs appeared in the center of the visual field of the stimulated eye and expanded at a rate of 70 - 90°/s. For measuring the latency between the onset of whole-field visual

motion and excitatory input to tectal neurons (Fig. 5), a stationary grating was presented to the eye contralateral to the recorded neuron. The grating then moved for 0.5 s in a front-to-back direction at a speed of 750°/s. The onset of grating motion was detected with a photodiode placed in the visual stimulation pathway and sampled at 10 kHz on the same A/D-board as the single-cell recording to precisely measure latencies between stimulus onset and synaptic responses. Visual stimuli were programmed using Python based OpenGL VisionEgg Software[75].

Analysis of electrophysiological data: Electrophysiological data were analyzed offline using LabView and MATLAB scripts. Peripheral motor nerve recordings were rectified by calculating the standard deviation in a 10-ms moving window, low-pass filtered at 500 Hz and median-subtracted. Fictive swim bouts were identified in the smoothed record using a threshold criterion of typically 4 standard deviations (SD) in each trace. The number of peaks exceeding the threshold ('bursts') and their location was measured in each trace. The average peak distance was taken as interburst interval. The difference between last and first peak location plus one interburst interval was taken as bout duration. The location of the first peak in the two traces, whichever came first, was taken as swim onset. Unilateral swim power ($Power_{ipsi}$, $Power_{contra}$) in a bout was measured in each of the two recordings as the area under the smoothed curve within the calculated bout duration. The summed swim power ($Power_{ipsi}$ + $Power_{contra}$) was taken as a measure of swim strength. To infer the direction of the swim, a direction index was calculated as ($Power_{ipsi}$ - $Power_{contra}$)/($Power_{ipsi}$ + $Power_{contra}$), with positive values indicating a swim directed towards the stimulus, ipsilateral to the stimulus position.

To quantify motor-related inhibitory synaptic currents in tectal neurons, the voltage clamp recording was baseline-subtracted using its mean in a 0.2 s-interval before swim onset. The charge transfer was calculated by integrating the recorded current trace in a window starting 50 ms after swim onset for 250 ms. When analyzing spontaneous swims, cells without discernible phasic IPSCs clustered around 0 pC charge transfer (Fig. 2C), and were taken as receiving no motor-related inhibition. Cells that exhibited sharp rising, phasic IPSCs typically had charge transfer ≥0.8 pC. IPSC onset was measured as the time of crossing a threshold of typically 3 SD in the current trace, from which the IPSC delay relative to swim onset was measured. The

delay between onset of whole-field image motion on the retina and excitatory inputs in tectal cells (Fig. 5) was determined correspondingly.

To measure motor-related voltage signals, swim-triggered voltage traces were baseline subtracted and averaged for each cell, from which a cross-cell average and SEM-trace were calculated (Fig. 1E). Visually evoked spiking activity was quantified by identifying spikes using a rate of rise criterion ≥5 mV/ms to determine spike times (Fig. 4). Assuming that the spike output from the recorded population of cells converges on a single premotor target, a population spike count was calculated (Fig. 4B,F) in bins of 100-ms. For each cell, the average number of spikes across trials was calculated for each bin and summed across cells. Spike frequency was calculated as the inverse of average spike count in each bin for each cell (Fig. 4E). For determining the time-resolved spike probability (P_{spike}, Fig. 4G) for cells that receive motor-related inhibition vs. those that do not, the summed spike count histogram was determined for each group separately and divided by the total number of spikes.

Morphological analysis: Following electrophysiological recording, a dual color image stack of the recorded neuron and the surrounding GFP-labeled structures in the *Tg(pou4f1-hsp70l:GFP)* background was acquired. GFP-fluorescence bleed-through was subtracted from the red channel sub-stack. Image stacks were cropped where no structures of the recorded neuron were detectable to remove background fluorescence from spilled indicator and to better bring out the position of GFP-positive tectal layers near the recorded neuron. To analyze dendritic morphology, image stacks were rotated to obtain a side view of the recorded neuron. Line profiles were taken from each color channel separately of the maximum intensity projection of the rotated stack, peak-scaled. The red and green channel line profiles from all recorded cells were then aligned with respect to the PVL/neuropil boundary and the center of the SFGS fluorescence, and averaged (Fig. 7).

Ca2+ imaging

Data acquisition: For Ca2+ imaging of swim-related activity in the tectal neuropil, zebrafish larvae were anesthetized using 0.02% MS-222 and then immobilized by incubation in α-bungarotoxin as described above. The larva was mounted, dorsal side facing upward, in a cylindrical recording chamber filled with embryo medium. Ca2+

imaging was performed using a multiphoton laser scanning microscope (Olympus FluoView FV1000), equipped with a water immersion objective (Olympus 20x/1.0 NA) and coupled with a Ti-Sapphire laser at an excitation wavelength of 920 nm. Emission light was filtered with a band-pass (515-560 nm). During imaging of tectal activity, spontaneous fictive motor activity was recorded unilaterally from the tail using a suction electrode as described above.

Spontaneous Ca2+ signals in the tectal neuropil were recorded in the dark, in multiple sweeps per larva, lasting 300 s each. At a depth of 30 µm from the dorsal most point of the tectum, a rectangular scan region (approx. 100 µm x 10 µm) covering all layers of the tectal neuropil was selected. Imaging was performed at a spatial resolution of typically 320 by 32 pixels, with a frame rate of 9-11 Hz. The fast scan direction was along the long axis of the rectangle. Spontaneous motor nerve activity was acquired at 10 kHz using LabVIEW. Ca2+ imaging and motor nerve recordings were synchronized using a trigger programmed in Python.

Analysis of Ca2+ imaging data: Ca2+ imaging and MNR data were analyzed using MATLAB scripts. Fictive swimming activity was automatically detected using the *findpeaks* function on the cubed and rectified MNR signal. Analysis was performed on isolated swim bouts, separated from preceding and following swim events by at least 3 seconds. Swims occurring within 10 s of turning on the laser were excluded, as well as motor nerve activity lasting less than 150 ms or more than 500 ms. The first peak of a selected swim bout was taken as swim onset.

To analyze localized Ca2+ signals in the tectal neuropil, the scanned rectangular region was subdivided into a regular grid of regions-of-interest (ROIs). Each ROI covered a square of approx. 2.8 µm x 2.8 µm of the scanned region, with shared edges between adjacent ROIs. For each individual ROI, the raw fluorescence time course was extracted and detrended using a quadratic fit. Fluorescence time course in each ROI was then expressed as $\Delta F/F = (F(t) - F_0) / F_0$, where F(t) is the fluorescent intensity at a given time point and F_0 is the mean of the lowest 50 F(t) values.

After alignment with the MNR recording, for each detected swim a 9 s time window with the swim onset taken as the midpoint was cropped out from the $\Delta F/F$ traces for each ROI and subjected to an automatic Ca2+ transient detection method, if the

following criteria were met: (1) a peak in the ΔF/F-trace of >2 SD was detected; (2) the duration of the peak was larger than 600 ms (peak duration defined by where the ΔF/F trace rose above its median level before and fell below it after the peak location). For ROIs in which these criteria were met, a Ca2+ response function defined by

C_0 x [1-exp(-(t-t_0)/τ_1)] x [exp(-(t-t_0)/τ_2], was fitted to the peak in the ΔF/F trace, with C_0, t_0 and τ_2 being free parameters. ROIs in which the correlation coefficient between the fitted and the measured signal exceeded 0.65 were considered 'active ROIs'. Ca2+ transient onset was taken as the interpolated time point at which the fitted response crossed its 10% level. The difference between Ca2+ transient onset and swim onset (Δt) was taken to classify Ca2+ transients as 'pre-swim' (Δt < -50 ms) or 'post-swim' (Δt > 50 ms). For shuffled control data (Fig. 6D), each recorded fluorescence sweep was circularly shifted by a random time interval chosen from a uniform distribution. The analysis was then done in the same way as for the original data. The shuffling process was repeated 15 times, from which the average histogram was calculated (Fig. 6D).

Immunohistochemistry

Immunohistochemistry: Larval zebrafish (5 dpf) of *Tg(pou4f1-hsp70l:GFP)* were anesthetized and transferred to 4% paraformaldehyde (PFA) in phosphate buffer saline (PBS) overnight at 4°C. Subsequently, the tissue was washed in PBS. Non-specific binding sites were blocked by incubation of the tissue in blocking solution (5% normal goat serum (Sigma, G6767), 1% blocking reagent (Roche, 11096176001), 1% bovine serum albumin (Sigma, A3059) in PBS containing 0.1% Tween 20, 1% DMSO) for 2 h at room temperature. Whole brains were incubated with anti-GFP (chicken anti-GFP, 1:500, Invitrogen A10262) and anti-$GABA_A$ (mouse anti-$GABA_A$ receptor β2,3 chain, 1:100, Merck MAB341). To visualize specific binding of the primary antibodies, the tissue was rinsed with buffer and incubated in secondary antibodies overnight at 4°C. GFP (anti-chicken 488 (1:1000), Invitrogen A11039) and $GABA_A$ (anti-mouse 546 (1:1000), Invitrogen A11003) was detected with appropriate secondary antibodies conjugated to Alexa Fluor dyes. Finally, the tissue was rinsed in PBS and mounted in mounting medium (80% glycerol, 1% agarose in PBS) for further analysis.

Analysis: Whole mount imaging of the immunolabelled tectal hemispheres was acquired using a laser scanning confocal microscope (FluoView 1000, Olympus) with a water-immersion objective (Olympus 20x/1.0 NA). Green fluorescence was excited at 488 nm, red fluorescence was excited at 561 nm. Images were acquired with a spatial resolution of 1024x1024 pixels. Confocal images were processed in ImageJ: Rectangular ROIs (width: 40 µm, length: 55 to 120 µm) were defined ranging from the PVL/neuropil boundary to the dorsal boundary of the tectal neuropil, at comparable depths across all samples. A median-filtered image of the ROI was subtracted from the raw image. The processed ROI was thresholded using maximum entropy thresholding. For the quantification of stained puncta the Analyze Particle command was used. Particles greater than 8 pixels and a circularity of more than 0.3 where counted as immuno-labeled puncta. To account for differences in neuropil extent across samples, neuropil depth was normalized to 100%, binned in 10 % steps. For the 10 subregions, the proportion of puncta in every bin was calculated by dividing the number of puncta in each spatial bin by the sum of puncta across all bins.

Acknowledgment

We thank Margit Böhler and Harald Noeske for expert technical help, and Sabine Götter for excellent help with fish husbandry. We thank Andrew Straw for comments on an earlier version of the manuscript and Wolfgang Driever and members of the Driever and Bollmann lab for helpful discussions. JHB thanks Winfried Denk for support. We thank Hitoshi Okamoto and the National Bioresource Project of Japan for providing the *Tg(pou4f1-hsp70l:GFP)* line. This work was performed with support from the Max Planck Society and the German Research Association (DFG; Project-Nr. 357057764, 398417145, 453632629 and 357057560).

Author Contributions

MAA, KL, SJP, CAT and JHB designed experiments. MAA, KL, SJP and CAT performed experiments. MAA, KL, SJP, CAT and JHB analyzed data. JHB wrote the manuscript with help from MAA and KL and feedback from CAT and SJP.

Competing Interests

The authors declare no competing interests.

REFERENCES

1. Masland RH. The neuronal organization of the retina. *Neuron* 2012;76(2):266-80.
2. Crapse TB, Sommer MA. Corollary discharge across the animal kingdom. *Nat Rev Neurosci* 2008;9(8):587-600.
3. Wurtz RH. Corollary Discharge Contributions to Perceptual Continuity Across Saccades. *Annu Rev Vis Sci* 2018;4(1):215-37.
4. von Holst E, Mittelstaedt H. Das Reafferenzprinzip. *Naturwissenschaften* 1950;37(20):464-76.
5. Sperry RW. Neural basis of the spontaneous optokinetic response produced by visual inversion. *J Comp Physiol Psychol* 1950;43(6):482-9.
6. Fukutomi M, Carlson BA. A History of Corollary Discharge: Contributions of Mormyrid Weakly Electric Fish. *Front Integr Neurosci* 2020;14:42.
7. Bell CC. An Efference Copy Which Is Modified by Reafferent Input. *Science* 1981;214(4519):450-53.
8. Poulet JF, Hedwig B. The cellular basis of a corollary discharge. *Science* 2006;311(5760):518-22.
9. Pichler P, Lagnado L. Motor Behavior Selectively Inhibits Hair Cells Activated by Forward Motion in the Lateral Line of Zebrafish. *Curr Biol* 2020;30(1):150-57.e3.
10. Richmond BJ, Wurtz RH. Vision during saccadic eye movements. II. A corollary discharge to monkey superior colliculus. *Journal of Neurophysiology* 1980;43(4):1156-67.
11. Sommer MA, Wurtz RH. A pathway in primate brain for internal monitoring of movements. *Science* 2002;296(5572):1480-2.
12. Thiele A, Henning P, Kubischik M, et al. Neural Mechanisms of Saccadic Suppression. *Science* 2002;295(5564):2460-62.
13. Bremmer F, Kubischik M, Hoffmann KP, et al. Neural dynamics of saccadic suppression. *J Neurosci* 2009;29(40):12374-83.
14. Kim AJ, Fitzgerald JK, Maimon G. Cellular evidence for efference copy in Drosophila visuomotor processing. *Nat Neurosci* 2015;18(9):1247-55.
15. Fenk LM, Kim AJ, Maimon G. Suppression of motion vision during course-changing, but not course-stabilizing, navigational turns. *Curr Biol* 2021;31(20):4608-19.e3.
16. Fujiwara T, Cruz TL, Bohnslav JP, et al. A faithful internal representation of walking movements in the Drosophila visual system. *Nat Neurosci* 2017;20(1):72-81.
17. Kramer DL, McLaughlin RL. The behavioral ecology of intermittent locomotion. *American Zoologist* 2001;41(2):137-53.
18. Dunn TW, Mu Y, Narayan S, et al. Brain-wide mapping of neural activity controlling zebrafish exploratory locomotion. *Elife* 2016;5:e12741.
19. McElligott MB, O'Malley DM. Prey tracking by larval zebrafish: axial kinematics and visual control. *Brain Behav Evol* 2005;66(3):177-96.
20. Bianco IH, Kampff AR, Engert F. Prey capture behavior evoked by simple visual stimuli in larval zebrafish. *Front Syst Neurosci* 2011;5:101.
21. Trivedi CA, Bollmann JH. Visually driven chaining of elementary swim patterns into a goal-directed motor sequence: a virtual reality study of zebrafish prey capture. *Front Neural Circuits* 2013;7(86):86.
22. Mearns DS, Donovan JC, Fernandes AM, et al. Deconstructing Hunting Behavior Reveals a Tightly Coupled Stimulus-Response Loop. *Curr Biol* 2020;30(1):54-69.e9.
23. Bollmann JH. The Zebrafish Visual System: From Circuits to Behavior. *Annu Rev Vis Sci* 2019;5:269-93.
24. McLean DL, Fan J, Higashijima S, et al. A topographic map of recruitment in spinal cord. *Nature* 2007;446(7131):71-5.
25. Gabriel JP, Trivedi CA, Maurer CM, et al. Layer-specific targeting of direction-selective neurons in the zebrafish optic tectum. *Neuron* 2012;76(6):1147-60.
26. Koyama M, Minale F, Shum J, et al. A circuit motif in the zebrafish hindbrain for a two alternative behavioral choice to turn left or right. *Elife* 2016;5:e16808.

27. Masino MA, Fetcho JR. Fictive swimming motor patterns in wild type and mutant larval zebrafish. *J Neurophysiol* 2005;93(6):3177-88.
28. Ahrens MB, Li JM, Orger MB, et al. Brain-wide neuronal dynamics during motor adaptation in zebrafish. *Nature* 2012;485(7399):471-7.
29. Kitamura K, Judkewitz B, Kano M, et al. Targeted patch-clamp recordings and single-cell electroporation of unlabeled neurons in vivo. *Nat Methods* 2008;5(1):61-7.
30. Aizawa H, Bianco IH, Hamaoka T, et al. Laterotopic representation of left-right information onto the dorso-ventral axis of a zebrafish midbrain target nucleus. *Curr Biol* 2005;15(3):238-43.
31. Sato T, Hamaoka T, Aizawa H, et al. Genetic single-cell mosaic analysis implicates ephrinB2 reverse signaling in projections from the posterior tectum to the hindbrain in zebrafish. *J Neurosci* 2007;27(20):5271-9.
32. Temizer I, Donovan JC, Baier H, et al. A Visual Pathway for Looming-Evoked Escape in Larval Zebrafish. *Curr Biol* 2015;25(14):1823-34.
33. Dunn TW, Gebhardt C, Naumann EA, et al. Neural Circuits Underlying Visually Evoked Escapes in Larval Zebrafish. *Neuron* 2016;89(3):613-28.
34. Nikolaou N, Lowe AS, Walker AS, et al. Parametric functional maps of visual inputs to the tectum. *Neuron* 2012;76(2):317-24.
35. Rupprecht P, Carta S, Hoffmann A, et al. A database and deep learning toolbox for noise-optimized, generalized spike inference from calcium imaging. *Nat Neurosci* 2021;24(9):1324-37.
36. Ahrens MB, Orger MB, Robson DN, et al. Whole-brain functional imaging at cellular resolution using light-sheet microscopy. *Nat Methods* 2013;10(5):413-20.
37. Romano SA, Pietri T, Perez-Schuster V, et al. Spontaneous Neuronal Network Dynamics Reveal Circuit's Functional Adaptations for Behavior. *Neuron* 2015;85(5):1070-85.
38. Northmore DP. Holding visual attention for 400millionyears: A model of tectum and torus longitudinalis in teleost fishes. *Vision Res* 2017;131:44-56.
39. DeMarco E, Tesmer AL, Hech B, et al. Pyramidal Neurons of the Zebrafish Tectum Receive Highly Convergent Input From Torus Longitudinalis. *Front Neuroanat* 2021;15:636683.
40. Anzelius M, Ekstrom P, Mohler H, et al. Immunocytochemical localization of the GABAA/benzodiazepine receptor beta2/beta3 subunits in the optic tectum of the salmon. *J Recept Signal Transduct Res* 1995;15(1-4):413-25.
41. Folgueira M, Sueiro C, Rodriguez-Moldes I, et al. Organization of the torus longitudinalis in the rainbow trout (Oncorhynchus mykiss): an immunohistochemical study of the GABAergic system and a DiI tract-tracing study. *J Comp Neurol* 2007;503(2):348-70.
42. Sadamitsu K, Shigemitsu L, Suzuki M, et al. Characterization of zebrafish GABAA receptor subunits. *Sci Rep* 2021;11(1):6242.
43. Bell CC, Han V, Sawtell NB. Cerebellum-like structures and their implications for cerebellar function. *Annual Review of Neuroscience* 2008;31:1-24.
44. Severi KE, Portugues R, Marques JC, et al. Neural Control and Modulation of Swimming Speed in the Larval Zebrafish. *Neuron* 2014;83(3):692-707.
45. Keller GB, Mrsic-Flogel TD. Predictive Processing: A Canonical Cortical Computation. *Neuron* 2018;100(2):424-35.
46. Ibbotson MR, Cloherty SL. Visual perception: saccadic omission--suppression or temporal masking? *Curr Biol* 2009;19(12):R493-6.
47. Avitan L, Pujic Z, Molter J, et al. Behavioral Signatures of a Developing Neural Code. *Curr Biol* 2020;30(17):3352-63 e5.
48. Kubo F, Hablitzel B, Dal Maschio M, et al. Functional architecture of an optic flow-responsive area that drives horizontal eye movements in zebrafish. *Neuron* 2014;81(6):1344-59.
49. Henriques PM, Rahman N, Jackson SE, et al. Nucleus Isthmi Is Required to Sustain Target Pursuit during Visually Guided Prey-Catching. *Curr Biol* 2019;29(11):1771-86 e5.

50. Fernandes AM, Mearns DS, Donovan JC, et al. Neural circuitry for stimulus selection in the zebrafish visual system. *Neuron* 2020
51. Heap LAL, Vanwalleghem G, Thompson AW, et al. Luminance Changes Drive Directional Startle through a Thalamic Pathway. *Neuron* 2018;99(2):293-301 e4.
52. Heap LA, Vanwalleghem GC, Thompson AW, et al. Hypothalamic Projections to the Optic Tectum in Larval Zebrafish. *Front Neuroanat* 2017;11(135):135.
53. Yokogawa T, Hannan MC, Burgess HA. The dorsal raphe modulates sensory responsiveness during arousal in zebrafish. *J Neurosci* 2012;32(43):15205-15.
54. Filosa A, Barker AJ, Dal Maschio M, et al. Feeding State Modulates Behavioral Choice and Processing of Prey Stimuli in the Zebrafish Tectum. *Neuron* 2016;90(3):596-608.
55. Tay TL, Ronneberger O, Ryu S, et al. Comprehensive catecholaminergic projectome analysis reveals single-neuron integration of zebrafish ascending and descending dopaminergic systems. *Nat Commun* 2011;2:171.
56. Filippi A, Mueller T, Driever W. vglut2 and gad expression reveal distinct patterns of dual GABAergic versus glutamatergic cotransmitter phenotypes of dopaminergic and noradrenergic neurons in the zebrafish brain. *J Comp Neurol* 2014;522(9):2019-37.
57. Heap LA, Goh CC, Kassahn KS, et al. Cerebellar output in zebrafish: an analysis of spatial patterns and topography in eurydendroid cell projections. *Front Neural Circuits* 2013;7:53.
58. Folgueira M, Riva-Mendoza S, Ferreno-Galman N, et al. Anatomy and Connectivity of the Torus Longitudinalis of the Adult Zebrafish. *Front Neural Circuits* 2020;14:8.
59. Hibi M, Shimizu T. Development of the cerebellum and cerebellar neural circuits. *Dev Neurobiol* 2012;72(3):282-301.
60. Bae YK, Kani S, Shimizu T, et al. Anatomy of zebrafish cerebellum and screen for mutations affecting its development. *Dev Biol* 2009;330(2):406-26.
61. Harmon TC, McLean DL, Raman IM. Integration of Swimming-Related Synaptic Excitation and Inhibition by olig2(+) Eurydendroid Neurons in Larval Zebrafish Cerebellum. *J Neurosci* 2020;40(15):3063-74.
62. Knogler LD, Kist AM, Portugues R. Motor context dominates output from purkinje cell functional regions during reflexive visuomotor behaviours. *Elife* 2019;8:e42138.
63. Robles E, Smith SJ, Baier H. Characterization of genetically targeted neuron types in the zebrafish optic tectum. *Front Neural Circuits* 2011;5:1.
64. Berman RA, Cavanaugh J, McAlonan K, et al. A circuit for saccadic suppression in the primate brain. *J Neurophysiol* 2017;117(4):1720-35.
65. Miura SK, Scanziani M. Distinguishing externally from saccade-induced motion in visual cortex. *Nature* 2022;610(7930):135-42.
66. Straschill M, Hoffmann KP. Activity of movement sensitive neurons of the cat's tectum opticum during spontaneous eye movements. *Experimental Brain Research* 1970;11(3):318-26.
67. Chen CY, Ignashchenkova A, Thier P, et al. Neuronal Response Gain Enhancement prior to Microsaccades. *Curr Biol* 2015;25(16):2065-74.
68. Savier EL, Chen H, Cang J. Effects of Locomotion on Visual Responses in the Mouse Superior Colliculus. *J Neurosci* 2019;39(47):9360-68.
69. Phongphanphanee P, Mizuno F, Lee PH, et al. A circuit model for saccadic suppression in the superior colliculus. *J Neurosci* 2011;31(6):1949-54.
70. Idrees S, Baumann MP, Franke F, et al. Perceptual saccadic suppression starts in the retina. *Nat Commun* 2020;11(1):1977.
71. Isa T, Marquez-Legorreta E, Grillner S, et al. The tectum/superior colliculus as the vertebrate solution for spatial sensory integration and action. *Curr Biol* 2021;31(11):R741-R62.
72. Basso MA, Bickford ME, Cang J. Unraveling circuits of visual perception and cognition through the superior colliculus. *Neuron* 2021;109(6):918-37.

73. Lister JA, Robertson CP, Lepage T, et al. nacre encodes a zebrafish microphthalmia-related protein that regulates neural-crest-derived pigment cell fate. *Development* 1999;126(17):3757-67.
74. Akerboom J, Chen TW, Wardill TJ, et al. Optimization of a GCaMP calcium indicator for neural activity imaging. *J Neurosci* 2012;32(40):13819-40.
75. Straw AD. Vision egg: an open-source library for realtime visual stimulus generation. *Front Neuroinform* 2008;2:4.